Summer Programs Symposium

August 4th – August 5th, 2021

Abstract Booklet

Summer Program for Undergraduate Research (SPUR)

Trevor Stiede - Wisconsin Lutheran College
Ross Collery, PhD
Department of Ophthalmology and Visual Science

Analysis of zebrafish irbp and irbp-like

Background

Myopia is the most common visual disorder in the world affecting over 20% of people over 40 inthe US. Myopia can often lead to other visual deficiencies such as glaucoma, cataract, retinal detachment, and macular degeneration. Mutations in human interphotoreceptor retinoid-binding protein (IRBP) are associated with myopia and retinal degeneration. However, its role in preventing retinal degeneration andmaintaining emmetropization of the eye is not well understood. During evolution, the irbp gene in zebrafish has been duplicated resulting in irbp and irbp-like. Together, these genes account for the expression profile and roles of IRBP in humans. To determine the effects of the irbp-like gene in zebrafish, we will compare the relative refractive error in zebrafish with and without the absence of
irbp-like. As well as use irbp transgenic fish to identify interacting protein partners.

Methods

CRISPR/Cas9 technology was used to delete irbp-like in the zebrafish eye. Optical coherence tomography (OCT) then took place at 3 weeks and 4 weeks post-fertilization. OCT images were used to calculate the relative refractive error in each eye of the fish. Genotyping of these fish then proceeded.

To investigate potential interacting partners of Irbp, transgenic gnat2:irbp-eGFP zebrafish wereused. Immunoprecipitation of GFP-tagged proteins attempted to identify co-precipitating interacting partners.

Results

The average ratio between lens diameter: body length, axial length: lens diameter, and axial length: body length all decrease from 3 weeks to 4 weeks. Axial length:lens diameter and axial length: body length ratios were significantly different between wild-type and heterozygous *irbp-like* mutants. Nosignificant change in relative refractive error was observed between irbp-like heterozygotes and wild- types. No novel interacting partners were identified following immunoprecipitation of Irbp-eGFP or Irbp- like-eGFP.

Conclusion

In conclusion, data trends shown to be insightful as all data was trending towards significance from 3 weeks to 4 weeks. Further OCT and analysis will also be completed at 7 weeks to expand the data overtime. Research for the identification of interacting protein partners of Irbp and Irbp-like will also be continued with alternative strategies such as cell culture techniques.

Sophie Boutouis – University of Texas at Dallas

Julia Dickson-Gomez, PhD
MCW Institute for Health & Equity

A qualitative exploration of reasons for seeking treatment among people who use opioids

Background
The opioid epidemic remains one of America's most pressing crises, with an estimated 93,331 Americans dying from drug overdoses in 2020 during the COVID-19 pandemic – an approximate 30% increase from 2019. While public health responses are largely focused on eliminating systemic or structural barriers to treatment, seeking treatment is ultimately a drug user's choice. This research expands on the literature by exploring the factors that lead people who use opioids (PWUO) to enroll in drug treatment services.

Method
The current study is part of a larger project that aims to compare the effects of opioid-related laws and policies in Connecticut, Kentucky, and Wisconsin on the transitions from prescription opioids to heroin, fentanyl, and/or injection drug use. Study teams in each state conducted in-depth, semi-structured interviews with 121 participants who use heroin or prescription opioids nonmedically. Participants were selected using a purposive sampling strategy. Interview questions regarded reasons for drug use and/or treatment, facilitators and barriers to treatment, stigma, and availability of treatment and harm-reduction services. Interviews were coded using MAXQDA software to allow for thematic content analysis of the data.

Results
The findings showcase that PWUO have various reasons for seeking treatment. More specifically, the results illustrate three global themes and six themes: motives related to friends and family (either *for* them or *because of* them), quality of life (lack of personal fulfillment or adverse health consequences), and the law (regarding the legal system or money). Interviewees with intrinsic versus extrinsic motivations and/or a large support system also expressed more positive attitudes toward treatment.

Conclusion
The results demonstrate that PWUO seek treatment for different reasons, but those who enter treatment voluntarily generally express more optimistic feelings toward recovery. Further research is needed to determine whether intrinsic or extrinsic motivations are more effective in keeping people in treatment and having more positive outcomes. Since some drug users still would not get treatment even if common barriers like cost, stigma, and transportation were eliminated, understanding how and at what pivotal moments PWUO decide to seek help can assist lawmakers in creating meaningful opioid policies and getting more people into treatment.

Keywords
Opioid epidemic, prescription opioids, heroin, drug treatment

Wolu Chukwu – Minerva Schools at KGI

Marja T. Nevalainen, MD, PhD and Lavannya Sabharwal, PhD

Department of Pathology

Title: Epidermal Growth Factor Receptor (EGFR) family expression in prostate cancer cell lines.

Background

The Epidermal Growth Factor Receptor (EGFR) family - comprising the members ErbB1, ErbB2/HER2, ErbB3/HER3, and ErbB4/HER4 - belongs to a large category of Receptor Tyrosine Kinases that phosphorylate proteins within cells. These receptors mediate pathways such as RAS-ERK MAPK, PI3K-AKT, JAK/STAT that induce cell proliferation and inhibit apoptosis, thus underscoring their roles as proto-oncogenes.[1,2] The upregulation of EGFRs and the constitutive activation of its downstream signaling pathways has been confirmed in various cancers including non-small-cell lung cancer, breast cancer, glioblastoma, pancreatic, and colorectal cancer.[1] ErbB2, for example, interacts with Janus kinase 2 (Jak2) despite its intrinsic tyrosine phosphorylation to induce tumorigenesis in breast cancer.[3] While this mechanism has been extensively characterized, its potential role in prostate cancer cells that also exploit the JAK/STAT signaling pathway in tumorigenesis remains to be elucidated. Therefore, we hypothesize that EGFR family members induce cell-proliferation and anti-apoptosis through JAK/STAT signaling in prostate cancer cells. For preliminary studies, we investigate the endogenous expression of the EGFR family in different prostate cancer cell lines.

Methods

LNCaP, DU145, and CWR22Rv1 prostate cancer cells were grown in their respective media and harvested with scrapping buffer containing phosphatase inhibitors. Cell pellets were lysed using cell lysis buffer (CLB) supplemented with protease inhibitors (pepstatin, aprotinin, leupeptin and PMSF). Samples (protein lysate + CLB + loading buffer) were run on SDS-PAGE gels with β-Actin as the loading control. Gels were transferred to the blotting membrane using the iBlot2 dry transfer system. Membranes were blocked to prevent unspecific binding and exposed to primary antibodies – EGFR (sc-120, mouse), ErbB2 (sc-08, mouse), ErbB3 (sc-283, rabbit), ErbB4 (sc-8050, mouse) – overnight, washed, and subsequently treated with anti-mouse (and anti-rabbit for ErbB3) secondary antibodies.

Results

Our results were inconclusive as we detected no bands of EGF receptor family proteins across all the prostate cancer cell lines. However, there were bands of lower molecular weight proteins that showed unspecific binding. Our inability to detect ErbB family members could have resulted from the weakness of the primary antibody used rather than an absence of these proteins from the cell lines. Even bands of actin confirmed uniform protein loading across wells.

Conclusion

We are unable to ascertain the endogenous (or lack of) of EGF Receptor family members in CWR22Rv1, DU145, and LNCaP prostate cancer cell lines. Moving forward, this experiment could be repeated using new ErbB family antibodies that are more potent at binding to the protein. Such an experiment yielding results confirming the endogenous expression (or absence) of EGFR family members in prostate cancer cell lines provide motivation for further experiments on the role of Jak/STAT signaling in prostate cancer and potential targeted therapies.

References

1. Wee P, Wang Z. Epidermal growth factor receptor cell proliferation signaling pathways. *Cancers(Basel)*. 2017;9(5):52.
2. Oda K, Matsuoka Y, Funahashi A, Kitano H. A comprehensive pathway map of epidermalgrowth factor receptor signaling. *Mol Syst Biol*. 2005;1(1):2005.0010.
3. Yamauchi T, Yamauchi N, Ueki K, et al. Constitutive tyrosine phosphorylation of ErbB-2 viaJak2 by autocrine secretion of prolactin in human breast cancer. *J Biol Chem*. 2000;275(43):33937-33944.

Uchechi Jennifer Nworah- Mississippi Valley State University.
Stephanie Olivier-Van Stichelen, PhD
MCW Department of Biochemistry

Characterizing the Degradation of OTX2 by the Ubiquitin-Proteasome System and Autophagy.

Background: The *O*-GlcNAc post-translational modification of nuclear, cytoplasmic, and mitochondrial proteins is reversible and dynamic. It is the addition of one N-acetylglucosamine to serine/threonine residues, catalyzed by the enzyme *O*-GlcNAc Transferase, and hydrolyzed off proteins by *O*-GlcNAcase (OGA). *O*-GlcNAc regulates many cell processes including transcription, translation, cell cycle, and protein degradation. It also plays an important role in early development and diseases such as cancers, diabetes, and neurodegenerative diseases. The critical developmental transcription factor and major oncogene in medulloblastoma, Orthodenticle homeobox 2 (OTX2), is heavily modified by *O*-GlcNAc. While the function of this modification in regulating OTX2 is unknown, our lab has previously shown that OTX2 was stabilized with increased levels of overall O-GlcNAcylation in mouse and cell models. A combination of proteasome inhibition (MG-132 mediated) and increased *O*-GlcNAc (OGA inhibitor Thiamet-G mediated) overnight led to further stabilization of OTX2 compared to MG-132 treatment alone, suggesting an alternative mode of degradation of OTX2. We hypothesize that OTX2 protein degradation is regulated by UPS and autophagy, and my summer project consisted of investigating this through drug treatments in various lengths and combinations.

Methods: A620 medulloblastoma cells, which express OTX2 through a gene duplication, were treated with Thiamet-G (OGA inhibitor, 100nM), MG-132 (2uM), and Chloroquine (autophagy inhibitor, 50uM) for different times (2, 8, 24 and 48 hours) before protein lysate harvest. OTX2 levels were then assessed by SDS-PAGE and Western blotting, normalizing to Actin levels. A follow up experiment involved all possible combinations of the drugs for an 8hr treatment.

Results: We observed an increase in OTX2 for all individual drugs at 8hr treatments, with Chloroquine showing the greatest OTX2 stabilization when compared to the vehicle control. OTX2 levels at the 2hr treatments were the same for all drugs except Thiamet-G, which showed a slight decrease. There was a consistent decrease in OTX2 levels for all individual drugs at 24hrs of treatment. We observed a slight decrease in OTX2 at 48hr for Thiamet-G. Additionally, we obtained no signal for OTX2 or Actin from cells treated with MG-132 or Chloroquine for 48hrs, suggesting cell death upon this long-term treatment.

Conclusion: The results obtained suggest that OTX2 can be degraded through autophagy in addition to the proteasome. This form of dual and cooperative degradation has been shown for other early developmental transcription factors and oncogenes such as SOX2, OCT4, and NANOG. Additional replicates of this experiment are required to validate the findings, and we are in the process of normalizing the results from the combination of drug treatments.

Keywords: Orthodenticle homeobox 2 (OTX2); O-linked N-acetylglucosamine (*O*-GlcNAc); Proteasome; Autophagy.

Ethan Lane – St. John Fisher College
Gustavo Leone, PhD; Anthony Trimboli, PhD
MCW Department of Biochemistry

Probing Stromal/Epithelial Interaction in the Mouse Mammary Gland

It has been determined that cells adjacent to the tumor (collectively called stroma) can affect the initiation, growth, and/or progression of the tumor. PTEN, a known tumor suppressor in epithelial cancers cells, is an example of a protein that can influence mammary epithelial growth through stromal expression. Therefore, it stands to reason that there are other gene products produced by stromal cells that could influence epithelial tumor progression. Stromal gene candidates were generated by a C. elegans genetic screen. These candidate genes were then assessed *in vivo* through a Cre-loxP knockout system in mice. Here we show that genetic deletion of two of these candidates together, Tlk1/2, in the mammary stroma were able to effect mammary gland morphology, but not when deleted in mammary epithelial cells. However, their loss in the stroma did not enhance or delay epithelial tumor growth with the overexpression of the epithelial tumor driver ErbB2 (neu). This suggests that Tlk1/2 in stromal cells do not have a role in the mammary gland for neu oncogenesis.

Angela Zhou - University of California, Berkeley
Brian Volkman, PhD
MCW Department of Biochemistry

NMR-Based Screening of Chemical Fragment Libraries to Identify Novel Ligands for the Tumorigenic Chemokine CCL28

Background

CCL28 is a chemokine expressed in the epithelial cells of most mucosal tissues, and there is strong evidence that it plays a key role in the creation and maintenance of an immunosuppressive tumor microenvironment. In response to tumor hypoxia, CCL28 stimulates the chemotactic migration of myofibroblasts and various types of lymphocytes to the tumorigenic site, including regulatory T-cells, by activating the G protein-coupled receptor CCR10. Regulatory T-cells limit antitumor immune responses by suppressing the activation and proliferation of CD4+ helper T cells and CD8+ cytotoxic T cells, while also promoting angiogenesis. Stromal myofibroblasts generate a strong extracellular matrix that acts as a barrier to block out antitumor drugs and immune cells. The combined effects of these mechanisms indicate that tumor cells can facilitate positive growth and proliferation via the secretion of CCL28. The objective of this study is to identify a handful of small fragments that may be used in the eventual synthesis of a small-molecule inhibitor for CCL28. This small-molecule inhibitor, in theory, will prevent CCL28 from binding to CCR10 and ultimately prevent the generation of a tumorigenic microenvironment.

Methods

The fragments were identified via fragment-based drug discovery (FBDD), which involves the synthesis of a drug molecule from small chemical fragments that loosely bind to the target protein. 1,332 total fragments from the Targetmol and Enamine chemical libraries were screened using 2-dimensional nuclear magnetic resonance (NMR) screening. Specifically, CCL28 samples were synthesized using isotopic 15N, and NMR data on the cross-peaks between 1H and 15N were collected and analyzed to determine which fragments resulted in the most significant peak shifts. Fragments from both libraries were tested against CCL28 following a 12-plex to 3-plex to individual screening sequence. Successful hits were carried forward to be screened in the subsequent level. One of the final individual hits was NMR titrated in increment concentrations against 50 μM CCL28 to determine specific sites of interaction and their corresponding binding affinity.

Results

Five individual hits were identified as possible lead compounds for the development of a small-molecule CCL28 inhibitor (Figure 1). NMR titration of one of the hits from the Enamine library (SMILES code: Cc1cc(Cl)ccc1S(=O)(=O)Nc1ccon1) identified I53 and R52 as the two residues of the CCL28 polypeptide sequence with the greatest binding affinity for the titrated fragment (K_d values of 3.3 mM and 6.3 mM, respectively) (Figure 2).

Figure 1.

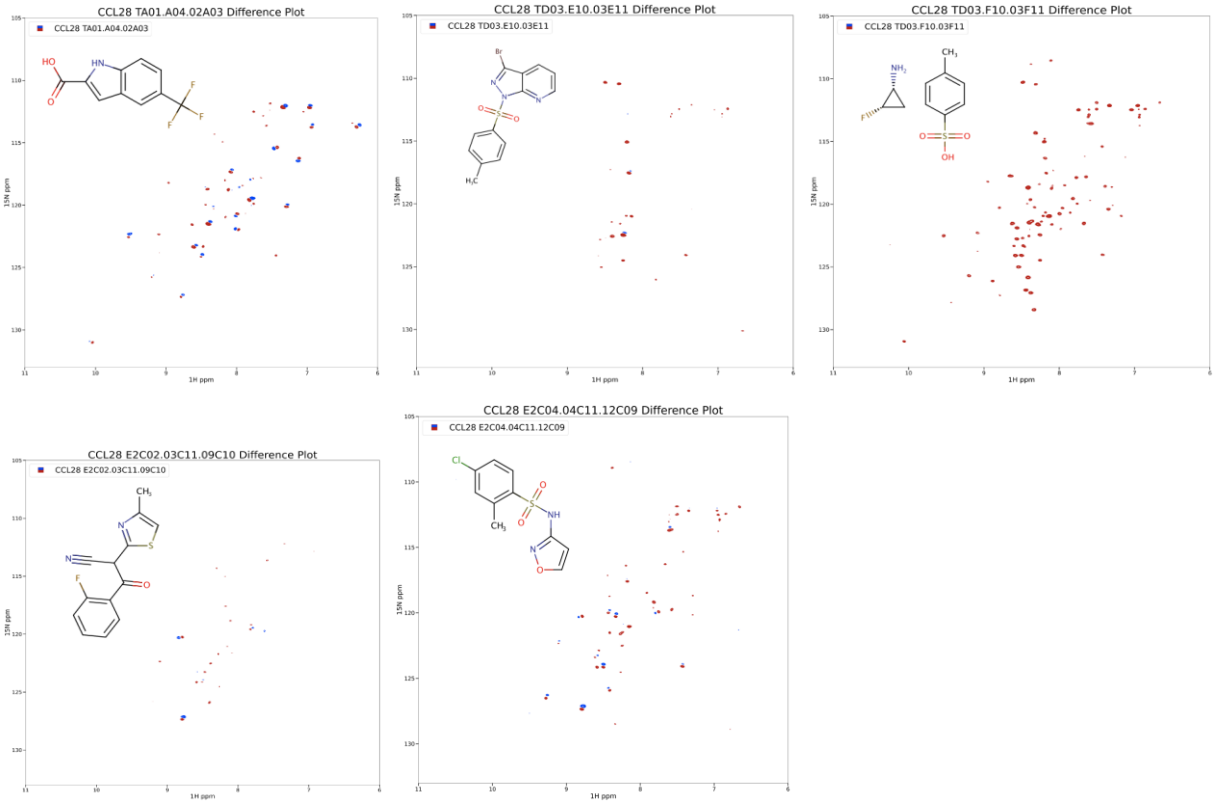

Figure 2.

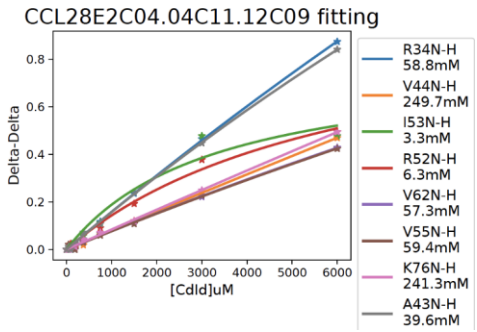

Conclusion

The results of this project demonstrate the viability of 2D NMR-based fragment screening as a method for FBDD. Immediate next steps include determining the binding affinities of the remaining four hits via NMR titration. Fragment(s) with the highest affinity can then be used to begin synthesizing a small-molecule inhibitor for CCL28.

Keywords: CCL28; fragment-based drug discovery (FBDD); pancreatic ductal adenocarcinoma; nuclear magnetic resonance (NMR)

Charles Met - University of Rochester
Dr. Raul Urrutia, MD
MCW Genomic Sciences and Precision Medicine Center (GSPMC)

Distinct K-Ras Variants Uniquely Alter Signaling Pathways Essential in Pancreatic Oncogenesis

Pancreatic cancer persists as a highly lethal disease due to a lack of notable external symptoms in early-stage patients (1). Consequently, pancreatic cancer is usually detected during later stages of disease and has initiated metastases, hindering the likelihood of patient survival (1). Inadequate early-detection methods and high patient mortality rates establish a heightened need for the development of post-diagnostic treatment. Studies have indicated that the Kirsten rat sarcoma viral oncogene protein (K-Ras) may be of particular interest to therapeutic efforts, finding it undergoes somatic point mutations in roughly 90% of pancreatic cancer cases (2). Belonging to the Ras protein family, K-Ras is a GTPase that participates in several signal transduction pathways that influence cell division, differentiation, metabolism, and apoptosis when activated by GTP (3). When mutated, the hot spot mutations existing at amino acid positions 12 and 13, the K-Ras protein is unable to properly hydrolyze GTP to GDP (2). Consequently, K-Ras remains improperly activated, the extent of which is based on the specific amino acid substitution (2). This erroneous activity of K-Ras is thought to contribute to cellular deviations from homeostasis, provoking oncogenesis (3). My research aimed to more specifically evaluate this premise by determining the impact common cancer-inducing K-Ras mutations have on the expression and phosphorylation of core proteins, both upstream and downstream, in K-Ras mediated pathways. In determining altered expression patterns, the role of K-Ras in causing pancreatic cancer can be better characterized. Human cells, containing mutated K-Ras proteins, were grown both in the presence and absence of doxycycline, an antibiotic which induces mutant K-Ras expression in these engineered cell lines. Cell lysates were obtained from these cultures to determine the levels and activity of various proteins of interest via Western Blot Immunodetection. Some proteins of interest included ERK, AKT, NFκβ, mTOR, and several others. The results of these assays were then quantified via a densitometry assay to display the directionality and consistency of the expression changes. It was confirmed that K-Ras overexpression alters the expression of other proteins in these critical transduction pathways and observed that the pathways are differentially impacted based on the specific K-Ras variant utilized.

Keywords: Pancreatic cancer, Somatic point mutations, K-Ras, GTPase, Signal transduction pathways, Lysates, Proteins, Oncogenesis, Western Blot Immunodetection

Sources:

1. "Pancreatic Cancer Prognosis." *Johns Hopkins Medicine*, www.hopkinsmedicine.org/health/conditions-and-diseases/pancreatic-cancer/pancreatic-cancer-prognosis.
2. Mann, Karen M., et al. "KRAS-Related Proteins in Pancreatic Cancer." *Pharmacology & Therapeutics*, Pergamon, 3 Sept. 2016, www.sciencedirect.com/science/article/pii/S0163725816301590?via%3Dihub.
3. Urrutia, Raul, et al. "Structural Bioinformatics Enhances Mechanistic Interpretation of Genomic Variation, Demonstrated through the Analyses of 935 Distinct RAS Family Mutations." *Bioinformatics (Oxford, England)*, Oxford University Press, 16 June 2021, www.ncbi.nlm.nih.gov/pmc/articles/PMC8208742/.

Tessa Shankey – Carroll University
Alexander Staruschenko, PhD
MCW Department of Physiology

Characterization of CIC-6 in Renal Nephrons Relating to Sodium Transport

Background

A leading global health concern is hypertension, which is linked to increased risk of heart attack, heart failure, renal failure, and stroke. Recent genome-wide association studies have linked *CLCN6*, which encodes the transport protein ClC-6, to blood pressure regulation; however, little is known about the function of this protein, and its role in renal ion transport has not been established. ClC-6 has variable expression along the nephron, where it is expressed in the proximal tubule (PT), thick ascending limb (TAL), distal convoluted tubule (DCT), and collecting duct (CT). A previous study by Flister et al. found that the *Clcn6* KO rats had reduced Na^+ and Cl^- excretion on a high salt diet. We hypothesized the loss of *Clcn6* will alter sodium transporter expression and activity in the PT, TAL, DCT, and/or CT.

Methods

To test this hypothesis, we quantified protein expression of key Na^+ transporters and channels and between Dahl Salt Sensitive rats with (WT) or without (KO) the *Clcn6* gene on either a high salt (4.0%) or normal salt (0.4%) diet. After tissue collection, lysates were prepared from kidney cortex tissue and Western blots were used to assess protein expression. Transporters were selected based on concordant localization with *Clcn6* along the nephron. In the PT, expression of the proteins: αNA/K-ATPase, SGLT2 GLUT2, and NHE3 was measured. In the TAL and DCT, NCC, pNCC, NKCC2, and pNKCC2 protein expression was assessed. Phosphorylated forms, denoted with a p, give an indication of the transporter activity levels. Lastly, in the CT, αENaC, βENaC, and ɣENaC levels were determined

Results

Among the normal salt and high salt diet rats, we did not observe any specific differences in protein expression of the PT or DCT Na^+ transporters; however, a significant decrease in NKCC2 and pNKCC2 in the TAL was observed. Additionally, there was a significant increase in α- and ɣENaC of the CT. No significant difference in βENaC was observed.

Conclusion

Our results are consistent with our hypothesis. There are statistically significant differences between KO and WT rats' Na+ transporter expression, specifically that of αENaC. Future studies may further interrogate and confirm these findings. Single channel patch-clamp analysis of CT tubules may determine whether loss of ClC-6 altered ENaC activity. An increase in ENaC expression may explain the decrease in Na+ excretion in the KO rats and point to a potential role for ClC-6 to help regulate renal Na+ transport in the distal nephron.

Keywords: *CLCN6*, ClC-6, Na+ transport, renal physiology, hypertension

Brie Forster – Carleton College
Anne Kwitek, PhD
MCW Department of Physiology

Sex Differences in Liver *Ugt1a9* Gene Expression in Heterogenous Stock Rat Founding Inbred Strains

Background

Analogs of bisphenol A (BPA), such as bisphenol F (BPF), are common BPA substitutes in manufacturing. Research indicates an association between BPF and adverse health effects in humans, including increased adiposity and endocrine disruption. UDP-glucuronosyltransferase 1a9 (Ugt1a9) is an enzyme expressed in the liver that is capable of metabolizing BPF. The Kwitek lab has identified a negative relationship between liver *Ugt1a9* expression and adiposity degree in male rats exposed to BPF, indicating that increased expression of BPF-metabolizing enzymes may protect the body by eliminating active chemicals. Additional research suggests that sex-related factors can influence human liver expression of *Ugt1a9*. Preliminary results from a current Kwitek lab study implicate sex and genetic background as factors that influence susceptibility to BPF exposure in rats, although the relationship between these factors and *Ugt1a9* expression is unknown. The goal of this project is to analyze *Ugt1a9* liver gene expression in weanling males and females from HS founding inbred rat strains to determine whether sex or genetic background influence *Ugt1a9* expression.

Method

Liver samples were previously harvested from male and female weanling ACI/EurMcwi (ACI), BN/NHsdMcwi (BN), F344/Stm (F344), and WKY/NCrl (WKY) rats. RNA was isolated using TRIzol and the RNeasy Mini Kit (Qiagen). cDNA was reverse-transcribed using the iScript cDNA Synthesis kit (Bio-rad). A *Ugt1a9* qPCR experiment with IDT assays was run using a whole-body Sprague Dawley (SD) rat sample as a positive control and *Gapdh* as the endogenous control gene. A second qPCR experiment was conducted to test *Actb* as an endogenous control. Results were calculated using the ΔΔCt method normalizing to the SD control. Final sample sizes for each sex and strain group were 6-7.

Results

Our findings indicate interstrain differences in *Gapdh* and *Actb* expression, making these genes poor controls for analyzing *Ugt1a9* expression differences between strains. There were no sex differences in *Gapdh* or *Actb* expression in any strain, which allows for sex-specific comparisons of *Ugt1a9* expression. F344 females showed increased *Ugt1a9* expression compared to their male littermates. No *Ugt1a9* expression differences were found between sexes in the other strains.

Conclusion

Our results suggest that *Gapdh* and *Actb* are poor controls for interstrain comparisons in these animals but are sufficient for intrastrain sex comparisons. Given their increased levels of *Ugt1a9* expression, F344 females may be less susceptible to the adverse effects of BPF exposure than males. Further experiments with a different endogenous control gene are required to assess interstrain variations in *Ugt1a9* expression.

Jose Acebedo – University of Illinois at Chicago
Paul Sylverster- Graduate Student
MCW Department of Microbiology

Rapamycin effect on mTOR and MHV-68 DNA synthesis

Gammaherpesviruses commonly affect humans, like the Epstein-Barr Virus (EBV) or the Kaposi's Sarcoma Herpes Virus (KSHV). EBV is the virus that causes mononucleosis, and by the adult age, almost everyone has antibodies to EBV, which show that they have previously been infected. KSHV is a common virus that causes Kaposi's Sarcoma (KS), but not everyone that has been infected will develop cancer. KS is more common in those who have been infected and have a weakened immune system or are immunocompromised. Another virus that is in the same family is the Murine Gammaherpesvirus-68 (MHV-68) which affects rodents. This is the virus used to model the natural gammaherpesvirus infection, for it is easy to manipulate the virus and the host, in vitro and in-vivo.

Kinase mTOR (mechanistic target of rapamycin) is responsible for cell growth, proliferation, and survival. It is also involved in anabolic processes, as well as lipid and DNA synthesis. Rapamycin is an acute inhibitor of mTOR, which phosphorylates the substrate S6 Kinase 1, responsible for protein synthesis and cell proliferation. Rapamycin inhibits the replication of human gammaherpesviruses in transformed cell lines and it inhibits the growth of human gammaherpesvirus-driven lymphomas. IN this project, KSHV infection is much more common than KS. Most people infected with this virus do not get KS and many will never show any symptoms. Infection with KSHV is needed to cause KS, but in most cases, infection with KSHV alone does not lead to KS. Most people who develop KS, have the KSHV, and they also have a weakened immune system, due to HIV infection, organ transplant, being older, or some other factor. To do this we looked that the macrophage derivation from bone marrow. Through a plaque assay, we were able to determine that rapamycin inhibits MHV-68 replication in primary macrophages. We ran a Q-PCR to look at the viral DNA at different time points. We found that rapamycin does not affect viral DNA synthesis.

Isabel Szablewski – Carroll University

Brian Smith, PhD

MCW Department of Biochemistry

BET Bromodomain Inhibitors Reduce Transcription of Proinflammatory Mediators in Macrophages

Autoimmune diabetes is mediated by chronic inflammation of the pancreatic islets. Activated macrophages within these islets produce and secrete proinflammatory cytokines such as interleukin 1β (IL-1β). High concentrations of IL-1β result in amplified transcription of inducible nitric oxide synthase (iNOS), an inflammatory mediator, within insulin-secreting β-cells in the islet, which results in accumulation of nitric oxide (NO) within β-cells. The prolonged presence of elevated NO levels leads to β-cell apoptosis and autoimmune diabetes. Recent studies have shown that the bromodomain and extra terminal domain (BET) family of proteins, a druggable class of epigenetic readers, may contribute to the onset and progression of autoimmune diabetes. The BET family has four members (BRD2, BRD3, BRD4, and BRDT) each containing two bromodomains (BD1 and BD2) and an extra terminal domain. Bromodomain proteins bind to acetylated residues of transcription factors and histones and recruit transcriptional machinery to facilitate the transcription of associated genes. Inhibition of both BD1 and BD2 by a pan-BET bromodomain inhibitor prevents type 1 diabetes in diabetic mouse models. We hypothesize BET proteins activate transcription of the inflammatory genes, IL-1β and iNOS, in macrophages. Additionally, we hypothesize that selective inhibition of only one of the BET bromodomains is necessary to both prevent and reverse the progression of autoimmune diabetes, which may avoid the toxicity seen in clinical trials of pan-BET bromodomain inhibitors. We show that BET bromodomain inhibition decreases the transcription of IL-1β and iNOS, iNOS protein levels, and nitrite (an oxidative metabolite of NO) concentration in a mouse macrophage cell line (RAW 264.7). RAW 264.7 cells were treated with two pan-BET inhibitors (IBET-151 and JQ1), two selective BD1 inhibitors (GSK-778 and GSK-789), and a selective BD2 inhibitor (GSK-046). IL-1β and iNOS transcription was analyzed using reverse transcriptase quantified polymerase chain reaction. iNOS protein levels were assessed by immunoblot. Nitrite concentration was determined by Griess assay. We show that selectively inhibiting BD1 in macrophages marginally inhibits inflammatory gene transcription whereas inhibition of BD2 does not inhibit inflammatory gene transcription. Furthermore, inhibition of both bromodomains by pan-BET bromodomain inhibitors completely abrogates lipopolysaccharide induced transcription of inflammatory genes in RAW 264.7 macrophages. We will work to corroborate these results across multiple macrophage cell lines and primary tissue.

Bonnie Jin – University of Wisconsin-Madison
Shi-Jiang Li, PhD,
MCW Department of Biophysics

The Significance of FMRI Biomarkers in The Early Diagnosis of Alzheimer's Disease

Background

Over five million Americans suffer from Alzheimer's Disease (AD), the most common form of dementia that affects memory, thought processing and behavior. There is currently no cure, and without it, the number of Americans that suffer from AD may rise to 13.8 million by 2050.
An important goal of biomedical research is to establish indicators, such as biomarkers, especially during early preclinical stages for early diagnosis and intervention. This way, future treatments could target the disease as early as possible before it damages the brain too much. Biomarkers are characteristics that indicate the presence of disease. For example, blood glucose levels are used to measure the effectiveness of diabetes medicine. This literature review is focused on functional magnetic resonance imaging (fMRI) biomarkers and the role they play in the early diagnosis of Alzheimer's Disease.

Methods

Scholarly articles from various journals and online sources were used to create a literature paper review of fMRI biomarkers regarding the early diagnosis of Alzheimer's Disease. Focus was placed on the work that has been accomplished by the Li Lab of the Medical College of Wisconsin.

Results

The earliest symptom of AD is known as mild cognitive impairment (MCI). This is a window where it is possible to detect and diagnose Alzheimer's Disease before significant brain damage has started. However, diagnosis is usually delayed by a couple years after the beginning of symptoms. This early detection is vital to the foundation of early diagnosis and treatment.

An unbiased classification system of validated biomarkers was introduced by the National Institute of Aging and Alzheimer's Association (NIA-AA) in 2016 that uses three types of biomarkers. It is known as ATN: cerebral B-amyloid deposition, pathologic tau, and neurodegeneration. Within fMRI biomarkers, there are those that belong to resting state fMRI and those that belong to task-based fMRI. In addition to advantages of fMRI biomarkers, there are also challenges that come with single imaging modalities.

An example of a resting state fMRI biomarker is the Li Lab's COSLOF index that could be used as a noninvasive quantitative marker for the preclinical stage of Alzheimer's Disease. For task-based fMRI, the Li Lab created a composite biomarker called the CARE index. It has shown to significantly correlate with disease severity and its use would help determine stages of AD on a more advanced level. It has also been tested to be highly accurate and can accurately predict which MCI individuals will develop into AD over a period of three years.

Conclusion

Overall, fMRI biomarkers are highly important in the early diagnosis of Alzheimer's Disease. Not only are there certain features that can only be detected through imaging, various types of fMRI biomarkers have been proven to be significant in mapping out the progression of Alzheimer's Disease.

Kaitlyn Andresen – University of Wisconsin- Parkside
Michaela Patterson, PhD
MCW Department of Cell Biology, Neurobiology and Anatomy

The Effect of *Runx1* Overexpression on Cardiomyocyte Proliferation

Background

In the United States, heart disease remains the leading cause of death, prompting increased focus on cardiac regeneration. More recently, attention has been turned toward cardiomyocyte (CM) proliferation, as these cells regulate heart contractile function. In adult mice, it is rare for cardiomyocytes to enter the cell cycle, and cytokinesis is even further limited. At adulthood, most cardiomyocyte growth is due to 2 processes: hypertrophy and endomitosis, or entering and exiting the cell cycle without karyokinesis or cytokinesis, leading to polyploid cardiomyocytes. Some CMs remain mononuclear diploid cardiomyocytes (MNDCMs), and higher frequencies of the MNDCM have been linked to improved outcomes following myocardial infarction (MI). The Patterson lab has validated that the gene *Runx1* influences the MNDCM population. *Runx1* is expressed in CMs during development and is upregulated in the CM following injury to the heart, but it is not expressed in uninjured adult CMs. It may also be linked to dedifferentiation, which could be a precursor for proliferation, and eccentric hypertrophy. In this experiment, we evaluated the effect that *Runx1* has on the CM cell cycle and cardiac regeneration following injury.

Methods

To address this question, we utilized tamoxifen-inducible MYH6 CreER to induce cardiomyocyte-specific *Runx1* overexpression in the mouse. Mice were subjected to myocardial infarction (MI) by means of coronary artery ligation. Mice were labeled with EdU, a marker of DNA synthesis, either via osmotic pump or injection following injury. To evaluate the heart function before and after injury, echocardiograms were performed. Contractile function, dilation, and wall thickness were assessed. Hearts were then harvested at either 14 or 28 days after injury and whole hearts or single cells were collected for further analysis. Immunofluorescence was used to evaluate cell cycle activity and cardiac morphology.

Results

Overexpression of *Runx1* in CMs after MI significantly increased cell cycle activity in CMs compared to $CreER^+$ controls at both 14 and 28 days post injury. Additionally, there were measurable amounts of CM cytokinesis after injury in animals overexpressing *Runx1,* compared to control animals which demonstrate no CM cytokinesis. *Runx1* was also shown to lead to dedifferentiation and cellular eccentric hypertrophy.

Conclusion

These results demonstrate that not only does *Runx1* overexpression contribute to increased cell cycle activity, but that it further leads to proliferation. In addition, it contributes to cellular eccentric hypertrophy and increased dedifferentiation. This implies that *Runx1* overexpression is linked to proliferation of cardiomyocytes and therefore cardiac regeneration. Our data reinforce prior studies in other cell types that identified *Runx1* as a novel influencer of the CM cell cycle. This has

implications for future treatments and provides a potential pharmaceutical target for mitigating the effects of cardiac injury.

Keywords
Cardiomyocytes, Runx1, Cardiac Regeneration

Bryan Hernandez- The University of Texas at El Paso
Lezi E, PhD
MCW Department of Cell Biology, Neurobiology, and Anatomy
Neuroscience Research Center

Age-associated neurodegeneration of interneurons in *C. elegans*

Neurodegeneration is the process by which neurons and neuronal connections progressively atrophy leading to loss of function. Neurodegeneration can be caused by external and internal factors such as toxins, viruses, and is present in diseases such as Alzheimer's and Parkinson's diseases. However, neurodegeneration is also caused by natural aging of which we are not aware of the specificities of its molecular mechanisms. With the present study, the intended goal is to create models that serve as a basis for future age-related neurodegeneration studies. The study used *C. elegans*, and identified morphological differences stemming from aging in specific neurons by employing *in vivo* imaging techniques, primarily widefield fluorescence microscopy and confocal imaging. Two independent sets of neurons were examined in the study, ALA and PVQ neurons, both interneurons involved in the motor function of the organism. ALA neurons were tagged with a translational green fluorescent reporter, in order to visualize the dense core vesicles (DCVs) in the neurite which are responsible for the transport and release of neuropeptides along the neuron. PVQ neurons were tagged with a transcriptional red fluorescent reporter, allowing for visualization of the neuron's shape. Worms were imaged on day 1 and 9 of adulthood, to gather data on any visible morphological changes, with day 1 being young adulthood and day 9 representing late adulthood. At the conclusion of the study, age-related morphological differences were observed in the ALA neurons. The average distance between DCVs was significantly larger in day 9 worms (11.63 um) compared to day 1 worms (4.88 um). Similarly, the number of DCVs per millimeter neurite is significantly different as day 9 worms (64.36 DCVs/mm neurite) had less DCVs compared to day 1 worms (103.44 DCVs/mm neurite). Statistical analysis (two-tailed Student's *t*-test) returned *P* values of <.01 for both sets of data. With the PVQ neuron, neurodegeneration was not observed in the age range chosen for the study, suggesting that the neuron deteriorates at a different speed compared to previous studied neurons, likely due to factors such as their individual function and molecular structure. Regarding ALA neuron, as age-dependent changes were observed, further studies would be needed to conclude whether these morphological changes also coincide with molecular or behavioral changes. Ultimately, through this the intended goal is to establish a reliable model that allows for future studies surrounding underlying molecular mechanisms of neurodegeneration.

Ritika Patel – Rensselaer Polytechnic Institute
Jonathan S. Marchant, MA, PhD
MCW Department of Cell Biology, Neurobiology, and Anatomy

Insight on Schistosome Ion Channel Sequences

Schistosomiasis is a neglected tropical disease caused by infection with parasitic worms known as schistosomes. This disease, affecting over 200 million people worldwide is vastly understudied. Currently, the only drug available to treat schistosomiasis is praziquantel (PZQ). PZQ causes contractions of the worm by interacting with an ion channel from the transient receptor potential melastatin family known as ($TRPM_{PZQ}$). There are many subfamilies and subtypes of TRP channels, and it is not known if other members of the schistosome melastatin (TRPM) subfamily beyond $TRPM_{PZQ}$ are praziquantel sensitive. Confirming the predicted sequences of other genes in the TRPM family to allow for their expression and functional profiling is the next step in examining their sensitivity to PZQ. To determine the sequence of each gene, primers were designed using the genomic predictions for each TRPM channel. Polymerase chain reactions (PCR) were executed, and the products were purified with a typical cloning protocol. Plasmids were sent for sequencing and the results were analyzed and compared to the original genomic predictions to screen for misannotations. When analyzing 4 TRPM gene sequences, it was found that 7 primer sets matched the predicted sequence with 100% accuracy, 3 had base pair differences with no impact on amino acid sequence, 4 had base pair differences that did impact amino acid sequence, and one primer set had a 12 amino acid deletion (n=4) when compared to the genomic database. Some channels showed a missing exon (Smp_000050), while others matched the predicted sequence with great accuracy (Smp_165170). Sequencing each TRPM gene can help create protein models and provide a basis for future work that will be instrumental in our understanding of how PZQ works; this will facilitate development of new drugs capable of treating schistosomiasis.

K**eywords: Schistosomiasis, Praziquantel, TRP Channels, Ion Channels**

---

[1]Park SK, Gunaratne GS, Chulkov EG, Moehring F, McCusker P, Dosa PI, Chan JD, Stucky CL, Marchant JS. (2019) The Anthelmintic Drug Praziquantel Activates a Schistosome Transient Receptor Potential Channel. *J Biol Chem* 294:18873–80. 10.1074/jbc.AC119.011093

Cameron Otto - Carroll University
Chris Olsen, PhD
MCW
Neuroscience Research Center/ Department of Pharmacology and Toxicology

---

Optimizing Video Analysis of Behavior to Compare Natural Reward Seeking in Spare Nerve Injury and Uninjured Mice

Chronic pain is an issue for many humans, yet variable and difficult to quantify. Rodents are a useful model for studying this behavior after a Spare Nerve Injury (SNI) introducing chronic pain. One behavior that requires further analysis is anhedonia, which a previous study in rats associates with SNI (Thompson et al., 2018). Investigating natural reward drivers in mice is necessary to extend this claim. We investigated if mice following this surgery showed behavioral differences associated with the natural reward sucrose compared to Wild-Type (WT) mice. Additionally, quality video recordings used for animal behavioral analyses are necessary to quantify results in several applications of behavior research. Manual analysis is inconsistent and arduous, and contemporary commercial software is expensive and inaccurate. We explored new free open-source software DeepLabCut (DLC) and SimBA (SA) which exhibit highly accurate animal tracking and data analysis. We assessed behavioral differences of the injured and uninjured mice by recording active/inactive nose pokes in drug self-administration, drug-seeking, and time spent in active/inactive regions. Throughout the study we assayed mechanical sensitivity via von Frey filaments to ensure maintenance of chronic pain in SNI mice compared to WT. To compare the accuracy of the commercial software Any-maze (AM) with DLC/SA, we compared mouse tracking data in D7 self-administration sessions. With identical videos and zones analyzed, we compared the recorded time spent in regions of interest over the 1-hour session. We found no statistically significant difference in the active/inactive nose pokes between the SNI and WT mice, nor in the total number of reinforcers earned. Both SNI and WT mice preferred active nose pokes over inactive pokes significantly but found no significant difference in the amount of time spent in the active or inactive zones. We found no significant difference in the average time spent measurements for the two software, but there were discrepancies in time measured. Ideally these results would be identical, but they differed by several minutes. Our findings for the sucrose self-ad, seeking, and time spent between SNI, and WT mice do not align with findings of anhedonia in rats with chronic pain. We do, however, find success in open-source software over commercial software. Analysis of the tracking in AM and DLC/SA showed several instances of failed tracking in AM where tracking is delayed or completely incorrect. DLC/SA very accurately tracked the mouse and the zone it was in. These findings suggest promising application of these software in further behavioral analysis.

Thompson, S. J., Pitcher, M. H., Stone, L. S., Tarum, F., Niu, G., Chen, X., Kiesewetter, D. O., Schweinhardt, P., & Bushnell, M. C. (2018). Chronic neuropathic pain reduces opioid receptor availability with associated anhedonia in rat. Pain, 159(9), 1856–1866. https://doi.org/10.1097/j.pain.0000000000001282

Maddy Morrissey – Marquette University
John Mantsch, PhD
MCW Department of Pharmacology and Toxicology

Contribution of Estrogen Receptor Beta in the Prelimbic Cortex to Sex Differences in Drug-Seeking

Background

Preventing relapse to drug use during abstinence is a critical goal for management of substance use disorders (SUDs). Currently, there are no FDA-approved pharmacological treatments that target relapse prevention, making this a critical unmet need. Additionally, it is unlikely that the development of a single type of intervention will be effective for all subpopulations of afflicted individuals and, as such, chronically understudied subpopulations demand investigation. Female users have been historically understudied, and yet sex differences between males and females are pronounced. Studies have demonstrated that males are more likely to use drugs first, with females having been characterized as even more vulnerable to relapse when compared to male counterparts. One obvious distinction between male and female users is the level of the circulating gonadal hormone estrogen, which is prevalent in high concentrations in females compared to males. Further, through investigation in the lab, we have determined that estrogen, when acting on estrogen receptor beta, can have pronounced effects on the prelimbic cortex, a brain region involved in decision-making and drug-seeking behavior. As such, my project this summer has been to further our understanding of estrogen effects on prelimbic cortical signaling that may contribute to significant sex-dependent differences in susceptibility to relapse between males and females.

Method

Male and female rats will receive venous catheters and guide cannula targeting PRL cortex and will go through the self-administration paradigm in an operant chamber. Once stable self-administration behavior is observed, rats will be tested daily for self-administration for two-hour sessions over 14 days. After which, rats will undergo extinction training. After completing the paradigm, the rats will go through reinstatement testing of response to IP injections of cocaine or vehicle in conjunction with PRL infusion of estrogen beta antagonist PHTPP or vehicle. Reinstatement tests include pretreatments of estrogen receptor inhibitors and systemic injections of a reinstating dose of cocaine in gonadally intact female and male rodents. Rats were tested multiple times for reinstatement with different doses of cocaine and antagonist combinations.

Results

We predict that while there will not be differences in male and female rats during cocaine self-administration or extinction, female rats will be more susceptible to coc-primed reinstatement as observed by reinstatement following administration of lower doses of cocaine in females compared to males. We also predict that in females, reinstatement will vary across the estrous cycle with the highest levels of reinstatement during proestrus when estradiol levels are elevated. We predict that both sex and phase differences in reinstatement will be prevented by micro infusions of estrogen beta antagonist PHTPP into prelimbic cortex. While we anticipate that PHTPP will reduce reinstatement in females but not males, it is possible since estrogen receptor beta is expressed in male PFC that effects on males will also be observed.

Conclusion

Heighted susceptibility to relapse in women is an unaddressed women's health issue. Understanding the neurobiological mechanisms/processes that selectively determine relapses susceptibility in women is important for the development of more effective individualized intervention strategies.

Lucy Keegan – Marquette University
Wojciech K. Janiewicz
John D. Imig, PhD
MCW Drug Discovery Center

Epoxyeicosatrienoic Acid Targeted Therapeutics Prevent Mesangial Cell Hyperproliferation in Diabetic Conditions

Diabetic Nephropathy is the leading cause of end-stage renal disease and is seen in approximately 30% of diabetic patients.[1] Hyperglycemia in diabetic patients causes hyper proliferation of mesangial cells and over secretion of extracellular matrix proteins which expands the mesangium and subsequently obstructs glomerular capillaries.[2] The obstruction of glomerular capillaries causes glomerular dysfunction, leading to the onset of diabetic nephropathy.[3] We hypothesized that manipulating epoxyeicosatrienoic acids (EETs) would prevent hyperglycemic induced mesangial cell proliferation. EETs are known to prevent kidney damage through their vasodilating and anti-inflammatory effects but are oxidized to an inactive form via soluble epoxide hydrolase (sEH).[4] EET analogs are synthetic and cannot be degraded allowing them to function in the presence of sEH. Inhibition of sEH with *t*-AUCB prevents the degradation of EETs allowing them to remain active. In this experiment, human renal mesangial cells (HRMC) were exposed to diabetic nephropathy hyperglycemic conditions (30mM glucose) and treated with potential therapeutic compounds. HRMC proliferation and viability were measured by an MTT assay. Hyperglycemic conditions increases HRMC proliferation by 30%. *t*-AUCB, a soluble epoxide hydrolase inhibitor (sEH-i), was the most effective in preventing hyperproliferation in hyperglycemic conditions and decreased proliferation to approximately 50%. 8,9-Epoxyeicosatrienoic acid (8,9-EET) analog also prevented hyperproliferation of hyperglycemic HRMCs, but less effectively than *t*-AUCB. The results of our studies demonstrate that increasing EETs especially with t-AUCB, effectively prevented hyperproliferation of mesangial cells in hyperglycemic conditions. These finding suggest that increasing EETs could be a potential therapeutic for diabetic nephropathy.

---

[1] Jingbo Zhou, Shu Zhang, Xinyi Sun, Yan Lou, Jinjing Bao, Jiangyi Yu,
Hyperoside ameliorates diabetic nephropathy induced by STZ via targeting the miR-499–5p/APC axis,
Journal of Pharmacological Sciences, Volume 146, Issue 1, 2021, Pages 10-20.

[2] Miller, Charles & Pozzi, Ambra & Zent, Roy & Schwarzbauer, Jean. (2014). Effects of High Glucose on Integrin Activity and Fibronectin Matrix Assembly by Mesangial Cells.. Molecular biology of the cell. 25. 10.1091/mbc.E14-03-0800.

[3] Jingbo Zhou, Shu Zhang, Xinyi Sun, Yan Lou, Jinjing Bao, Jiangyi Yu,
Hyperoside ameliorates diabetic nephropathy induced by STZ via targeting the miR-499–5p/APC axis,
Journal of Pharmacological Sciences, Volume 146, Issue 1, 2021, Pages 10-20.

[4] Imig, J. D., Hye Khan, M. A., Burkhan, A., Chen, G., Adebesin, A. M., & Falck, J. R. (2021). Kidney-Targeted Epoxyeicosatrienoic Acid Analog, EET-F01, Reduces Inflammation, Oxidative Stress, and Cisplatin-Induced Nephrotoxicity. *International journal of molecular sciences*, *22*(6), 2793. https://doi.org/10.3390/ijms22062793

Trisha Xiong – Mount Mary University
Adam S. Greenberg, PhD
MCW & Marquette University Department of Biomedical Engineering

The Effects of Odor Congruency on Visual Perception: A Pilot Study
Xiong, T., Elliott, L., Greenberg, A.S.

Background

Research has shown that smell dysfunction is a potential indicator of COVID-19 disease; thus, olfactory testing could be used to aid in early diagnosis. Although COVID-19 smell dysfunction research is ongoing, the possible cognitive effects are still unknown. This research aims to measure the effect of odor context on participants' ability to discriminate between visual images of edible and inedible items. Future plans will extend this research towards COVID-19 patients.

Method

Healthy volunteers participate through an online testing platform (http://Testable.org). We use odors from the University of Pennsylvania Smell Identification Test (UPSIT; Sensonics, Inc).

Each session begins with the standard UPSIT 8-item test: participants identify the correct odor by clicking on one of four visual images. They then rate the eight odors for familiarity, intensity, and edibility (scale = 1 to 9), and pleasantness (scale = -4 to +4).

During the congruency task, participants scratch a "z" pattern into a microencapsulated odorant patch, then sniff the odor while viewing an image. Participants press the "J" key on a keyboard if the image is edible, and the "K" key if the image is inedible. After eight practice trials, participants complete 128 trials divided into four randomized blocks, each containing three conditions: (1) identical congruent (8 trials/block) contains odors/images that represent the same item, i.e., chocolate odor and chocolate image; (2) categorical congruent (8 trials/block) contains odors/images of either edible or inedible non-identical items, i.e., chocolate odor and strawberry image; (3) incongruent (16 trials/block) contains odors/images with different edibility, i.e., chocolate odor and rubber tire image. A ten-second break between each trial allows for clearance of odorants from the nasal cavity. The total duration of each is approximately 30 minutes.

Results (Predicted)

We hypothesize that participants will more accurately identify edibility on odor-image congruent trials and perform less accurately on odor-image incongruent trials.

Conclusion

These data could be used as a control group against which to compare patients who have COVID-19 smell loss. We speculate that COVID-positive patients with smell loss will be unaffected by our odor-picture congruency manipulation, whereas COVID patients without smell loss will yield results similar to normal control subjects. This task is designed to be sensitive to long-term effects of cognitive decline in the olfactory domain which may persist after odor perception dysfunction has subsided.

Sher Bahadur – Dickinson College
Ryuma Tanaka, MD
MCW Department of Pediatrics: Hematology and Oncology

GD2 Target Validation in Pediatric Brain Tumors and scFv Antibody Development for CAR T cell Therapy in Medulloblastoma

Background

Pediatric brain tumors are the leading cause of cancer related mortality in children and medulloblastoma is the most common malignant pediatric brain tumor. Chimeric antigen receptor (CAR) T cell therapy is a promising mode of cancer treatment that utilizes T cells engineered to express specific antigen receptors to recognize and destroy cancer cells. GD2 is a target antigen of immunotherapy for neuroblastoma and its expression on pediatric malignant brain tumors including medulloblastoma by immunohistochemistry has been reported. Our first objective is to validate the expression of GD2 on the surface of pediatric brain tumor cells derived from patient tumors by flow cytometry.

Single chain fragment variable (scFv) is a fusion protein of the variable regions of an immunoglobulin with antigen binding capability. The scFv sequence will be incorporated into the structure of a CAR to manufacture anti-GD2 CAR T cells. scFv display is a method to develop scFv against protein antigens. GD2 is a polysaccharide, and it is unknown if scFv display will identify a GD2 specific scFv. Our second objective is to identify a GD2-specific scFv from a human scFv phage library display.

Methods

We applied combined enzymatic and physical dissociation to create single cell suspensions from patients' tumor samples. These cells were stained with antibodies and analyzed by flow cytometry for detection of selected surface antigens GD2, L1CAM, B7-H3, PDGFRα, IL-13Rα, HER2, and EphA2. A human scFv phage display was screened against human GD2 molecules fixed on plates. Selected phages were grown in bacterial cells, rescued with helper phage, concentrated by precipitation, and validated for GD2 binding by an ELISA assay.

Results

Flow cytometry data showed that embryonal brain tumor including medulloblastoma and atypical teratoid rhabdoid tumor (ATRT) cells are strongly positive for GD2, weakly positive for B7-H3 and L1CAM, and negative for EphA2, IL-13Rα, and HER-2. ELISA data showed that our scFv phage library panning against plated GD2 enriched the library for GD2-specific scFv clones.

Conclusion

Our flow cytometry results validate that GD2 is a good target antigen of CAR T-cell therapy for pediatric embryonal brain tumors. scFv phage display panning against plated non-protein antigen may be a useful method to identify scFv that can be used for design of CAR T cells.

Alexandra Dunker – Texas Christian University

Correlating CD30 Levels and Cytotoxicity & The Development of Anti-CD30 CAR-T Cells

Background and Significance

Immunotherapy is an emerging field that utilizes the body's immune system to treat cancer. One specific type of immunotherapy involves the incorporation of engineered antibodies and antibody fragments. Antibodies are proteins produced by the immune system to identify and destroy pathogens in the body. The Medin Lab has developed monoclonal antibodies against CD30, which bind different epitopes. CD30 is a surface protein involved in immune regulation. CD30 is predominantly expressed on the surface of many different cancers, with lower levels of expression observed on B and T cells. Since CD30 is largely limited to cancerous cells, the off-target effects of CD30 immunotherapy should be minimal. Two of the Medin Lab's anti-CD30 antibodies have been incorporated into two different therapies: bispecific antibodies and chimeric antigen receptor T cells (CAR-T). Bispecific antibodies are made of two different IgG antibodies, one recognizing CD30 and one recognizing CD3, found on T cells. These IgGs are bound together at the Fc regions via chemical conjugation. One way of delivering anti-CD30 bispecific antibody immunotherapy is to load them *ex vivo* onto bispecific antibody armed-activated T cells (BATs). CAR-T cells are cytotoxic T lymphocytes modified to express an engineered T cell receptor with an extracellular domain that can bind to CD30 on a cancer cell's surface and an intracellular domain that triggers cytotoxicity. CAR-T therapy is a cutting-edge technology primarily used for non-solid tumors with high success rates in getting patients to remain in remission with no additional treatments. Overall, there were two aims of this project: to determine the level of CD30 expression necessary for efficient CD30+ cell cytotoxicity, and to produce recombinant lentivirus (LV) particles and demonstrate their ability to produce functional anti-CD30 CARs following transduction of Jurkat cells.

Methods

To determine the level of CD30 required to induce cytotoxicity when using anti-CD30 BATs, a Phycoerythrin Fluorescence Quantitation Kit (Quantibrite Kit) was used to measure the relative level of CD30 expression on eleven cell lines: K562, OCI AML2, OCI AML2 LV CD30, RAJI, RAJI LV30, HEK 293T, HEK 293T LV CD30, SU-DHL-1, RPMI6666, RAJI LV CD30 G/L, and primary T cells. In cells that normally do not express CD30 (HEK 293T, OCI AML2, and Raji cells), CD30 LV was used to induce expression. Then, Cr^{51} release assays were performed to determine the levels of cytotoxicity that resulted after incubating the above cell lines with the anti-CD30/CD3 BATs. The measured cytotoxicity was correlated with the level of expressed CD30, as observed with the Quantibrite Kit, on the various cell lines to determine the minimum CD30 concentration needed to elicit efficient cytotoxicity.

With the aim of developing an anti-CD30 CAR-T therapy, a 50-plate LV prep was performed to generate anti-CD30 CAR-T LV. A qPCR assay was performed to determine the vector copy number and titer of the LV prep following infection of HEK 293T cells. Jurkat cells were then transduced with the anti-CD30 CAR-T LV at a multiplicity of infection (MOI) of 3. Surface expression of the CAR was tested by flow cytometry following staining for either Fab or Protein L. The transduced cells were incubated with either CD30+ or CD30- cells to investigate CAR-T functionality with ELISAs measuring secreted IL-2 and TNFα expression levels following stimulation.

Results

Quantibrite Kit analysis suggests that the Raji LV CD30, Raji LV CD30 G/L, HEK 293T LV CD30, OCI AML2 LV CD30, and SU-DHL-1 cell lines had medium, RPMI6666 and K562 cell lines had low, and Raji, OCI AML2, HEK 293T, and primary T cells had little to no CD30 expression on their cell surface. The Cr^{51} release assays showed that Raji LV CD30, Raji LV CD30 G/L, HEK 293T LV CD30, RPMI6666, SU-DHL-1, OCI AML2 LV CD30, and K562 showed relatively high levels of lysis, whereas Raji, HEK 293T, OCI

AML2, and primary T cells showed little to no lysis when incubated with T cells armed with CD3/CD30 bispecific antibodies. As expected, CD30+ cell lines, HEK 293T LV CD30, OCI AML2 LV CD30, Raji LV CD30, and Raji LV CD30 G/L, were found to have significantly higher levels of lysis when compared to their CD30- counterparts, and the CD30+ cell lines SU-DHL-1, K562, and RPMI6666 were found to have significantly higher levels of lysis when compared to primary T cells. These Cr^{51} release assay results appear to agree with what was observed with the Quantibrite Kit assays.

A qPCR assay of the LV prep following infection HEK 293T cells showed that 1.9×10^9 IU/mL of the anti-CD30 LV was harvested from the LV prep. Flow cytometry failed to show significant shifts in fluorescence which would have indicated high levels of transduction. ELISA results showed CAR transduced cells expressed high levels of IL-2, but IFN- γ was not detected.

Conclusion

The BATs showed high specificity to CD30+ cells. The relative CD30 levels observed with the Quantibrite Kit appear to match the levels of cytotoxicity measured by the Cr^{51} release assay. This association between CD30 levels and quantified cytotoxicity could allow for future predictions on how cytotoxic armed T cells will behave when they encounter new cell lines or even in *in vivo* models. This has implications for future treatments to ensure that the tumor cells will be destroyed while the normal bodily cells are spared by the BATs, and this allows for cancer treatments to be more tumor-specific than current methods.

The LV prep yielded a high level of anti-CD30 CAR LV. Preliminary findings failed to show high levels of surface expression of the CAR. However, observations from the ELISAs indicate high levels of specific engagement occurred with the successfully transduced cells. These results suggest that when the cells are transduced, the CARs are functional, but a higher MOI will likely be required for greater transduction levels. These early findings show promise that this anti-CD30 CAR therapy will be an effective therapy to treat CD30+ tumors.

Keywords: Immunotherapy, Bispecific Antibody, CAR-T, T-cells, Cancer, CD30

Jared Mayrand – University of Wisconsin – Parkside
Jeffrey A. Medin, PhD, MACC Fund Professor
MCW Department of Pediatrics

Production & Assessment of Lentiviral Gene Therapy for Sickle Cell Anemia.

Background

Sickle cell anemia (SCA) is an autosomal recessive disorder that results from a single nucleotide polymorphism in the gene encoding the hemoglobin beta subunit. The mutation produces a misfolded hemoglobin, that can polymerize, causing sickling. Millions of SCA patients worldwide are susceptible to pain crises and complications involving organ damage. Our goal is to use a lentivirus-based gene therapy to insert an improved beta-globin subunit (AS-3) into hematopoietic cells obtained from Townes SCA mice. These mice are ideal models for SCA because they lack the mouse alpha- and beta-globins but have their respective human forms. In this study we demonstrate the effective production of the lentivirus and describe an *in vitro* hypoxia assay by which transgene efficacy can be determined.

Method

Lentivirus production utilized HEK cells transfected with several delivery plasmids encoding for lentiviral particles and the transfer plasmid containing AS-3. Virus was collected and purified. A titer-based qPCR assay was performed with serial dilutions of virus following infection of HEK cells. *In vitro* hypoxia assays were performed in triplicate using blood from young (2-4 month) and old (6-8 month), male and female Townes mice of normal (AA), heterozygous (AS) and SCA (SS) genotypes. C57BL6/J (B6) mice were used as wild-type controls. Blood was diluted in a sodium metabisulfite solution, applied to a microscope slide and sealed. The slides were incubated at 37 ºC for 45 minutes. Images were obtained from three different places per slide, using a Zeiss Upright microscope under the 40x objective. One-hundred cells were counted per image to quantitate sickling using ImageJ.

Results

Our recombinant lentivirus was successfully produced and isolated from HEK cells, although the titer-qPCR determining the quantity of virus obtained will be performed in the future. The hypoxia assay revealed that sickling did not occur regardless of age within B6 or AA mouse blood under hypoxic conditions. Heterozygous mice had sickling occur at 0.5% ±0.5, while 72% ±21 of the cells from SS mice sickled under the same conditions. Male mice had a significant difference in average sickling (61% ±20), compared to females (82% ±8). There was no difference in sickling between age groups of the same gender. Homozygous SS mice after bone marrow transplant with AA stem cells had sickling occur at less than 1% per hundred cells.

Conclusion

The *in vitro* hypoxia assay sets a foundation for determining the percent of mouse blood cells that sickle. Whereas age was not a significant factor in causation of sickling, genotype was, as cells from SS mice sickled significantly more than any other genotype. Females featured significantly higher percent sickling compared to males in both young and old age groups. Sickling in homozygous SS mice was reduced by over 99% with a bone marrow transplant utilizing AA mouse stem cells. The

results of the assay can be utilized for future experiments to determine the effectiveness of the gene therapy.

Keywords: Gene therapy, Sickle cell anemia, Lentivirus, Townes Mice

Tyler Thompson – University of Wisconsin - Parkside
Nathan Schloemer, MD
Medical College of Wisconsin – Department of Pediatrics

Regulation of Sarcoma Lentivector-Induced IL-12 Production by Cellular Fate Control Activation or Irradiation

Background

Bone and soft tissue sarcomas account for 11-14% of childhood malignancies but outcomes remain poor compared to those of other childhood cancers. Previous work from this lab has shown that introduction of sarcoma cells following lentiviral (LV) transduction to produce Human Interleukin 12 (hu-IL-12) into humanized mice causes a targeted immune response mediated by Natural Killer (NK) cells to significantly restrict tumor growth. Unfortunately, there was also undesired systemic inflammation associated with the response. This study aims to reduce the systemic inflammation by decreasing the introduced sarcoma's expansion and corresponding hu-IL-12 production. We hypothesize that treatment with azidothymidine (AZT) to activate the human thymidylate kinase (TMPK) cell fate control system included in the lentivector, or irradiating cells before introduction will decrease systemic inflammatory side effects while still preserving the potent local immune response. We sought to determine the efficacy of our fate control system and/or radiation in limiting sarcoma expansion without inhibiting the sarcoma from producing hu-IL-12 that can elicit NK cell effector functions.

Methods

We plated non-transduced, sham-transduced, and LV/hu-IL-12-transduced 143B (osteosarcoma) and A673 (Ewing's Sarcoma) cells in variable concentrations of AZT. IL-12 production was followed serially and quantified by an enzyme-linked immunosorbent assay (ELISA). We irradiated A673 cells with varying doses of radiation to test its effect on cell viability/expansion and IL-12 production. IL-12 production was serially measured by ELISA as in AZT treatment. Cell replication and viability were assessed by flow cytometry with markers for apoptosis and cell death; expansion was assessed by flow cytometry with a marker for cell replication. We tested the functionality of transduced vs non-transduced sarcoma supernatants through NK92-mi exposure and subsequent interferon gamma (IFN-γ) production, quantified by ELISA.

Results

100 μM AZT gradually decreases hu-IL-12 production in A673 over time as desired; 500-1000 μM concentrations rapidly decrease hu-IL-12 production to 0 by day 10. AZT concentrations as high as 1000 μM did not decrease hu-IL-12 production in 143B. Both 25 Gray and 86 Gray rapidly decrease hu-IL-12 production to 0 by day 7. Both radiation doses also cause roughly 60% of cells to be dead or apoptotic by day 6. 25 Gray causes a significant reduction in cell division compared to non-radiated samples. Production of hu-IL-12 following 100 μM AZT treatment elicits a strong NK response after two weeks. Irradiation with either 25 Gray or 86 Gray prevents an NK response.

Conclusion

Treatment with 100 μM AZT gives our desired dose response curve in A673 and looks promising for in vivo trials with mice. Radiation with 25 or 86 Gray is too much because the sarcoma is killed too quickly to potentially elicit immune response.

Emma Van Why – Belmont University
Shubhangi Prabhudesai, PhD, Karthikeyan Thirugnanam, PhD, Ramani Ramchandran, PhD
MCW Department of Pediatrics

Role of Cilia Protein in Vascular Stability

Background

Primary cilia are non-motile cilia that play an important role in in our vascular system. For this research, we are interested in the primary cilia that make up the endothelial cells that line blood vessels.

Arl13b is a ciliary membrane protein that aids in lengthening cilia. When Arl13b is not present or has lost its function, it can lead to malformed cilia. These cilia are often shorter in length and lack the proper structures for normal cilia integrity. These malformed primary cilia are linked with loss of vascular integrity, and thus cerebral hemorrhages are possible. Additionally, a mutation of the p21-activated kinase 2a (Pak2a) gene can lead to cerebral hemorrhages in zebrafish. This indicates that a Pak2a mutation is also associated with vascular integrity.

It has recently been discovered that there is a strong correlation between ciliopathies and non-functioning Arl13b protein. From previous research, we know that Arl13b mRNA when injected Pak2a zebrafish embryos rescues the cerebral hemorrhage phenotype.

We hypothesize that embryos introduced to the Arl13b protein at 24 hours post fertilization (hpf) will have a better chance of a rescue. This is because the blood vessels in the brain have not yet formed at 24hpf. This would allow Arl13b a greater chance of inducing an effect on cerebral vascular integrity. However, because the blood vessels are already formed by 30hpf, introducing Arl13b 30hpf will likely not rescue those blood vessels.

Method

Pak2a mutant zebrafish were bred, and their embryos were injected with a heat-shock plasmid containing GFP and Arl13b. The embryos were then heat shocked either at 24hpf or 30hpf. At 52hpf, we counted the number of bleeders and non-bleeders in each clutch. The embryos were then prepared for western blots to determine the presence of GFP in the embryos.

Results

The embryos heat shocked at 24hpf showed a good sign of rescue, decreasing the number of bleeders by about 6%. However, the embryos heat shocked at 30hpf did not show a good sign of rescue showing little to no decrease in the number of bleeders.

Conclusion

The results from this experiment support the original hypothesis: Arl13b introduced at 24hpf will give embryos a better chance of a rescue, whereas the embryos introduced to Arl13b at 30hpf will likely not have a good chance of a rescue. To sum, zebrafish can be rescued by introducing Arl13b before cerebral angiogenesis. Future experiments could use this information to determine how Arl13b cilia induction is contributing to vascular stabilization.

Grace Gibson- Marquette University
Ranjan Dash, PhD
MCW Department of Biomedical Engineering

Computational Modeling of Mitochondrial Matrix Calcium Buffering and Calcium Dynamics

Background

Nanomolar levels of free calcium increase oxidative phosphorylation and ATP synthesis in mitochondria. However, high levels (micromolar) of free calcium cause mitochondrial dysfunction via the opening of the mitochondrial permeability transition pore (MTP). Thus, it is important to understand how calcium is regulated as well as how calcium regulates different processes within the mitochondrial matrix. Within the mitochondrial matrix, calcium is buffered by different calcium-binding proteins and by amorphous calcium phosphate formation. A previous computational model of mitochondrial bioenergetics and calcium handling used a static value to represent the matrix calcium buffering capacity, but it has been shown that there are at least two classes of calcium buffers that regulate free calcium concentration within the mitochondrial matrix. Therefore, a dynamic value would be better suited to represent matrix calcium buffering capacity.

Method

The purpose of this study was to quantitatively understand calcium dynamics within the mitochondrial matrix by integrating dynamic matrix calcium buffering with a previous model of mitochondrial bioenergetics and calcium handling. Under the assumption of rapid equilibrium for both reactions between calcium and the two calcium buffer classes, an equation for matrix calcium buffering capacity was made using the law of mass action and mass balance at equilibrium. This equation replaced the static value for matrix calcium buffering capacity in the ordinary differential equation for free calcium within the mitochondrial matrix. Model simulations were made and compared to existing experimental data relating free calcium concentration within and external to the mitochondria. The model was also used to re-analyze calcium dynamics and its effect on other functions.

Results

The resulting computational model did not fit the experimental data used to construct the previous model to the same accuracy as the static value for matrix calcium buffering capacity. The activity of the calcium uniporter (CU) that transports calcium into the mitochondrial matrix was increased to account for the increase in matrix calcium buffering power. The activity of the sodium calcium antiporter and sodium hydrogen antiporter was increased to counteract the significantly higher levels of calcium in the mitochondrial matrix.

Conclusion

The model incorporates the dynamic nature of calcium buffering within the mitochondrial matrix due to two calcium buffer classes. In our lab's experiments, the external calcium concentration is known. Thus, that concentration is used to understand the effect of calcium dynamics on mitochondrial function. However, it is not the external calcium concentration that regulates these functions within the mitochondrial matrix. It is most likely the free matrix calcium concentration. Therefore, this model could be used to simulate how matrix calcium affects functions within in the mitochondrial matrix

without directly measuring it in an experiment. To improve this model, more experiments focused on illuminating matrix calcium buffering dynamics could be beneficial.

References

---

[1] Dash, R. K. and Beard, D. A. (2008), Analysis of cardiac mitochondrial Na^+–Ca^{2+} exchanger kinetics with a biophysical model of mitochondrial Ca^{2+} handing suggests a 3: 1 stoichiometry. The Journal of Physiology, 586: 3267–3285. doi:10.1113/jphysiol.2008.151977

[2] Bazil JN, Blomeyer CA, Pradhan RK, Camara AKS, Dash RK (2013) Modeling the calcium sequestration system in isolated guinea pig cardiac mitochondria. Journal of Bioenergetics and Biomembranes, 45: 177-188. doi.org/10.1007/s10863-012-9488-2

Jackson Radandt — Marquette University
Aoy Tomita-Mitchell, PhD and Brandon Tefft, PhD
MCW Department of Biomedical Engineering

Functional analysis of iPSC-CMs derived from a familial case of HLHS

Background:
Hypoplastic Left Heart Syndrome (HLHS) is a severe congenital heart disease affecting development of the left ventricular outflow tract, including the left ventricle, mitral valve, aortic valve, and proximal aorta. The specific genetic etiology of HLHS is unknown, however variants in cardiac genes such as *NOTCH1*, *NKX2.5*, *ERBB4*, *HAND1*, *GJA4*, and *MYH6* have been associated with HLHS. Our laboratory discovered that rare, damaging variants in *MYH6* were significantly enriched in a cohort of HLHS patients at Children's Wisconsin (CW) / Medical College of Wisconsin. The *MYH6* gene encodes for a-myosin heavy chain (a-MHC), a contractile protein in the cardiac sarcomere. *MYH6* is expressed in the myocardium during cardiac development and is the predominant MHC isoform in the postnatal atria. We hypothesized that *MYH6* variants contribute to HLHS by altering strength, speed, and patterns of contraction in cardiomyocytes. To study the impact of *MYH6* variants *in vitro*, we utilized induced pluripotent stem cell-derived cardiomyocytes (iPSC-CMs) as a disease model. iPSCs were reprogrammed from skin biopsies of patients with HLHS carrying *MYH6* variants, as well as their heart-healthy family members.
Methods:
To determine whether the observed *MYH6* variants affect iPSC-CM contractility, we assessed variant-carrying iPSC-CMs using two methodologies: single-cell analyses and bulk cell analyses. At the single-cell level, endogenous contraction of iPSC-CMs was observed and measured using IonOptix. Bulk analysis of contractility was achieved through video recording of monolayer iPSC-CMs - endogenously contracting cells were filmed for a duration of at least three contractions, at both 100X and 200X magnifications. Videos were then run through MUSCLEMOTION, a contractility analysis software. MUSCLEMOTION calculates parameters including contraction amplitude and duration, contraction and relaxation time, as well as maximal contraction and relaxation velocities, allowing us to assess differences between wild type and *MYH6* variant-carrying iPSC-CMs. The specific goal of this project was to optimize MUSCLEMOTION settings in order to obtain consistent, reliable output.
Results:
We found that reproducible output could be obtained from MUSCLEMOTION by taking video recordings at 60 frames per second (fps) or higher, removing Gaussian blur, and adjusting the speed window to 3. Using these settings, preliminary differences in time-to-peak, peak amplitude, rate, as well as maximal contraction and relaxation velocities were observed at differentiation day 25 between cell lines.
Conclusions:
This demonstrates the feasibility of evaluating the impact of *MYH6* variants using an iPSC-CM model system. These contractile differences will be connected to patient phenotypes to better understand the development of *MYH6*-variant specific HLHS.
Keywords:
Contractility, Cardiomyocyte, CHD, Sarcomere

Daphne Zhu – Yale University
Yang Wang, MD PhD
MCW Department of Imaging Research

Longitudinal changes in dynamic functional connectivity after sports-related repetitive head impacts in high school football players

Background
Sport-related concussion has serious implications for youth involved in contact sports (CS). Additionally, repetitive head impacts (RHIs) that do not lead to concussion, which occur far more often, can lead damaging neurocognitive effects and pose risk for long-term pathophysiological outcomes. However, the mechanisms by which RHIs lead to brain injury over multiple CS seasons remain unknown. Prior research has found changes associated with one season of RHI exposure, but findings remain inconsistent, and there is a particular need for research on the accumulated effects of multiple CS seasons. The dynamic functional network connectivity (dFNC) method has emerged as a powerful approach to detect subtle brain changes due to RHIs. The present study followed non-concussed high school football players to investigate longitudinal changes in dFNC over two seasons.

Method
21 high school football players completed clinical evaluations and resting-state functional MRI scans using a combined multiband, multi-echo sequence before and after each season of two consecutive seasons. Dynamic functional connectivity was estimated, and dFNC strength was compared between timepoints.

Results
No diagnosed concussion occurred during the study period. No differences in clinical measures of brain function were found across all four timepoints. The dFNC analysis identified four recurring connectivity states using a sliding-window analysis. Paired t-tests revealed significant changes in dFNC strength over both one and two seasons; however, the total number of changes was highest in the two-season comparison. We additionally identified decreases in default mode network connectivity and increases in higher-order network connectivity.

Conclusion
These findings are indicative of accumulated effects of RHIs on functional connectivity patterns, even in the absence of clinical symptoms or diagnosed concussion. Longitudinal evidence suggests a shift from temporary alterations in primary functional networks to higher-order cognitive networks including attention, memory, and executive control. This study is the first to apply the dFNC approach to investigate alterations in functional connectivity over multiple seasons in high school CS athletes. The insights gained from the temporal dynamics of network connectivity have the potential to serve as biomarkers of accumulated neurological damage due to RHIs.

Skylar Bogardus – University of Nevada,
RenoAndrew Nencka, PhD
MCW Department of Radiology

IMAGE PROCESSING IN THE PREDICTION OF THE EFFICACY OF TRANSARTERIALRADIOEMOBLIZATION (TARE) TREATMENT USING CONVOLUTIONAL NEURAL NETWORKS

Background: Hepatocellular carcinoma (HCC) is usually diagnosed late in its run and has an average survival of under two years (1). Transarterial radioembolization (TARE) is a local treatment aimed at mitigating symptoms and slowing progression (1). Radiologically observable tumor response to TARE is delayed by over six months. This project is investigating how the combined data in the pre-treatment SPECT, CT, and MRI imaging can predict response to TARE so plans may be more proactively evaluated.As a component of this work, the liver must be segmented from clinical images for quantitative analysis. Manual segmentation is prohibitive due to the time that it takes. Herein we have optimized a deep neural network for the pre-processing of thousands of clinical imaging exams, which can enable the developmentof predictive models.

Method: Using late arterial axial CT images of a patient's pre-treatment and 1-month post-treatment scans,the V-Net Medical for TensorFlow algorithm [2] was used to build a model to segment the liver. Several models with varying combinations of hyperparameters were trained and the results were compared to findwhat model would most effectively segment the liver in an external training set [3] (129 training and 2 validation datasets). Hyperparameters investigated included batch size, number of epochs, learning rate, upscale/downscale block size and dimensions, seed, and input shape of the image. The V-Net was trained with the unique hyperparameters and the dice coefficient [3] was plotted. The resulting loss functions in validation data were compared to find the combination of hyperparameters that performed best. Each segmentation was viewed using Analysis of Functional NeuroImages (AFNI) where, in cases of error, it could be manually edited to be added to the training data and the neural network re-trained for more effective generalization to the acquired clinical data.

Results: The results of the loss function comparisons were analyzed to find the model with minimal signsof overfitting/underfitting, with a loss as close to zero as possible. Training the model with default parameters yielded validation loss to be 0.137692. Optimization was performed sequentially, with a grid search over combinations of batch size, learning rate, block size and dimensions, and input down-sampling,followed by optimization of training epochs for the best performing model across the range of 50-150 epochs. The best performing hyperparmeters included batch size 3, learning rate 0.0001, downsample blocksize 3 with dimensionality of 3, upsample block size 3 with dimensionality of 2, input image resampling to96x96x64, and 75 training epochs which yielded a validation loss of 0.11425064. With the optimal networkidentified; the next step is to perform manual quality assurance on masks resulting from its application to subsets of the clinical images of interest and re-run the trainings with the additional data, iterating until the network performs sufficiently.

Conclusion: The goal of this project is to utilize machine learning to pre-process data to predict treatmentresponse to TARE from pre-treatment imaging. Such information will aid radiologists in evaluating the efficacy of TARE prior to or shortly following treatment. This work demonstrates optimized training of a convolutional neural network as a key portion of the data curation process.

The work done in the development of this research project is central to the advanced prediction of TARE treatment outcomes, and it serves as a foundation for future machine learning based image processing at the Medical College ofWisconsin.

References

[1] Mendiratta-Lala, M., et al. (2020). MRI assessment of hepatocellular Carcinoma after Local-regional Therapy: A comprehensive review. *Radiology: Imaging Cancer*, *2*(1). https://doi.org/10.1148/rycan.2020190024 [2] NVIDIA. (2020, September 24). Version (20.06.2). *V-Net Medical for TensorFlow*. https://ngc.nvidia.com/catalog/resources/nvidia:vnet_medical_for_tensorflow [3]Carass, A., et al. Evaluating White Matter Lesion Segmentations with Refined Sørensen-Dice Analysis. Scientific reports, 10(1), 8242. https://doi.org/10.1038/s41598-020-64803-w

Claire Lois - Saint Louis University
Kevin Koch, PhD - MCW Department of Radiology
Automated Segmentation of Carpal Bones in Wrist MRI using Convolutional Neural Networks

---

Background: When injured, carpal bones are hypothesized to have abnormal patterns of movement. In order to enhance diagnostic techniques for assessment of wrist injury or degeneration, technology to enable kinematic tracking of carpal bones using MRI is being developed at the Medical College of Wisconsin's Center for Imaging Research. The specific deep learning application to this project applies a convolutional neural network that leverages data from manually segmented (identified) carpal bones within wrists to train an inference model that can automatically identify the same carpal bones in new wrist imaging datasets. These segmentations are then utilized within previously developed image-based tracking technologies to explore motion behaviors of individual carpal bones during normal wrist movements.

Methods: Complete data for 5 subjects were utilized for data augmentation seeding and neural network validation. Each dataset included one fixed position 3D MRI, and 2 dynamic movement 4D MRI's (split into 40 time points). The scaphoid, capitate, and lunate were both manually and semi-automatically segmented so that a mask of each was created. As deep learning requires substantial amounts of training data, these 5 static and 400 dynamic 3D image/mask sets were utilized to generate synthetic augmented training data. One static image set, and 20% of the dynamic images were randomly held out of the augmentation process for final neural network validation. Augmentation was performed using each "seed" MRI volume and its complementary bone mask, whereby each seed went through the following augmentation process: 1) random rotation (around 3 principle Euler rotation axes) between 0.2 and 6 degrees, 2) random elastic deformation, 3) random spotlight (bias) intensity field to the images. From the seed image/mask volumes, 5000 augmented images and masks were created for both the static and dynamic image sets. Using a selection of data from the augmentations, and the corresponding labeled masks, a vnet deep learning network was trained to segment and find the three carpal bones of interest. Conventional deep-learning performance measures were assessed on the validation and test data sets. This training process was repeated for each of the 3 bones in the fixed and dynamic positions.

Results:

Using the original and augmented data sets, a deep learning network was trained to find and mask the capitate, lunate, and scaphoid. Predictions using set aside data were done. Once the data was analyzed for the static images, it was found that the manual segmentations were the most accurate, semi automated were second, and the neural nets were less accurate. In the dynamic positions, we found that the images varied too much to train a net as simply and in order to utilize deep learning, more steps need to be taken in the future. While the images are able to be segmented with great accuracy using a semi automatic segmentation method, the deep learning nets are thus far unable to correctly mask the bones.

Conclusion: The goal of this project was to take 5 kinematic wrist MRI exams (each having 1 high resolution 3D static image set and 400 dynamic 3D time frames) and their paired manual segmentation data sets, utilize 80% of the data to synthesize large training datasets through data augmentation methods, and train a deep learning convolutional neural network that can automatically extract (segment) the scaphoid, lunate, and capitate carpal bones. This technology development project provides crucial processing capabilities required to support ongoing research work at the Medical College of Wisconsin that is developing tools to analyze dynamic wrist MRI exams.

Keywords: Machine Learning, Data Augmentation, Segmentation, MRI

Cassandra Naze – Marquette University
Peter S. LaViolette, PhD
MCW Department of Radiology

Quantitative Comparison of Prostate Histology Between Two Slide Scanners

Background

Whole slide imaging (WSI) has recently become popular as a way to analyze tissue samples quantitatively. To utilize this method, samples are collected after surgery or biopsy and are paraffin embedded, sliced and stained with a battery of agents, such as hematoxylin and eosin (H&E), and digitized using an automated slide scanner. Different stains cause certain segments of the tissue to appear in different colors. For example, in H&E-stained prostate tissue, the different segments, stroma, epithelium and lumen (SEL), appear in different colors because of their composition. The slide scanner saves each stained sample as large image files, which can then be annotated by pathologists or analyzed for research purposes. The goal of this study was to assess two different slide scanners to determine their ability to produce images consistent with one another, and to determine whether quantitative pathomic features of prostate histology differed significantly.

Methods

To evaluate possible differences and inconsistencies between the Huron TissueScope LE and Olympus VS120 slide scanners, metrics, such as root mean squared error (RMSE) and the structural similarity index (SSIM), were calculated to compare images from both scanners in several categories. Prostate tissue samples had been previously collected as part of an ongoing prostate cancer study, and nine total slides scanned on both scanners were analyzed (three patients total with three slides from each). Custom code was developed in MATLAB (Mathworks, Natick, MA) using the image processing toolbox and in-house functions to analyze the image pairs. Image files from the scanner were very large (up to 20 Gb), so most of the analysis was done on down-sampled, lower resolution images or smaller regions of the full-size, high-resolution images. Methods used to compare the images included image registration and pixel dimensions, color intensity and deconvolution into the dominant color channels, first order segmentation of tissue and second order textural features. Statistical analysis was performed on segmented regions and textural features. Significance was determined using a Student's paired t-test, where a P value below 0.05 was significant.

Results

The analysis of the nine whole-mount pairs showed significant difference in color intensities and contrast of the images from the different scanners, calculated in the difference between RGB histograms. Scanners acquired images at different resolutions, so the quality of the images was not the same. This was seen in the SSIM calculated for the whole-mount, averaging 0.785 across all slides, and for the individual tissue segments (SEL), averaging 0.994 across all slides for all segments. There was also a difference in the alignment of the images, seen in the RMSE calculated from selected alignment control points. The average across whole-mounts was 42.298 and was 0.344 across all segments. Statistical analysis showed that all calculations performed on the segmentation results (standard deviation, kurtosis, and entropy) proved to be significantly different across the whole-mounts between the scanners. For the second order features, mean epithelium size (mean epithelial area per gland) and mean cell fraction (mean percent of nuclei per total gland area of epithelium

without lumen) both showed to be significantly different, while several other features showed a wide variance.

Conclusion

In conclusion, we showed significant differences between WSIs collected on the Huron TissueScope LE and Olympus VS120 slide scanners both in image quality, color contrast, and in pathomic features calculated from the tissue. Further research on this topic should focus on understanding if pathologist annotations differ greatly due to image quality, affecting a potential following analysis or diagnosis due to slide scanner differences.

Jeff Rodriguez - Middlebury College
Peter S. LaViolette, PhD
MCW Department of Radiology

Computer-Aided Annotation of Digital Histology Assays

Background

Digitizing histology slides and annotating them can help researchers highlight features of primary brain tumors. Histology derived features that quantify the cell morphology and texture of slides combined with pathology annotations like tumor, non-tumor, and necrotic tissue can be integrated into histology database. Annotations may differ across specialists with differing degrees of experiences. For this reason, automating this task can aid pathologists and specialists in standardizing their diagnoses. We tested the hypothesis whether Classification Machine Learning Models trained on histological features could predict which areas of brain tissue are tumor, non-tumor, or necrotic tissue.

Methods

After autopsies, brains are fixed in formalin using 3D printed cages to protect from structural deformation, sliced axially in-line with the patient's last MRI using 3D printed slicing jigs. Extracted samples are then stained with hematoxylin and eosin (HE) to differentiate between the nucleus and cytoplasm of cells. Digital histology slides serve as the input to a Histomics workflow which can process slides and quantify structural heterogeneity of brain areas. Quantitative image analytic techniques known as "radiomics" can convert digitized slides into explorable data. The data processing pipeline tiles high resolution and annotated images into tiles of 1024 x 1024 pixels (px). Each tile was segmented by using color threshold techniques that detect the boundaries between cytoplasm and nuclei. 31 tile features were extracted using MATLAB. Consequently, using Pyradiomics, 93 nuclei features, 93 ECF features, and 93 cytoplasm features were concatenated with the tile features to give a total feature set of 310 per tile. A primary component analysis was used to select the 41 primary components, which are linear combination of features, that explain 95% of the variance in the data. Lastly, the annotated tiles were labeled into either non-tumor (UL), infiltrative tumor (IF), or necrotic tissue (NE). Classification models were fitted with the 41 primary components of eight slides, trained to predict if a tile was UL, IF, or NE. The models were trained with eight slides across two patients and validated with four slides of across two patients.

Results

Support Vector Machine models have the highest accuracy of 76%. This model can predict tumor with 61% accuracy, non-tumor with 88% accuracy, and necrosis with 11% accuracy.

Conclusions

The LaViolette lab has the largest primary brain cancer specific brain bank with a total of 94 brains. The process of annotating slides and coregistering them to MRI scans is a way to find the extent to which cancer has spread. Automating the task of annotating histology slides is beneficial and can reduce the 2 hours it takes specialists to annotate digital slides.

[Riley Nugent – Carroll University]
[Astrid Stucke, MD]
[MCW Department of Anesthesiology]

Histological Identification of the Caudal Medullary Raphe in Adult Rabbits

The sub study was part of our investigation into the brainstem locations of opioid-induced respiratory depression. We found that injection of opioid receptor antagonist naloxone into the parabrachial nucleus/Kölliker-Fuse complex, pre-Bötzinger complex (preBC), and caudal medullary raphe (CMR) completely reversed the effect of systemic opioids. This study was to histologically confirm the location of the CMR injections.

The study was approved by local animal care committee and conformed with NIH standards. New Zealand White rabbits were anesthetized, mechanically ventilated, paralyzed, and decerebrated. Brainstem respiratory activity was recorded from the phrenic neurogram. The preBC was functionally identified with bilateral AMPA injections (1). We injected fluorescent (5%,140 nL) beads into the bilateral preBC, at presumed caudal edge of the raphe pallidus (2mm caudal to preBC, midline, ventral surface), and presumed medial medullary raphe (3mm rostral of preBC, midline, and ventral surface). Animals were transcardially perfused with formaldehyde. Histological preparation involved sectioning 20um slices of brainstem between 2mm caudal to obex to 2mm rostral to the pons. Slices were stained for 4′,6-diamidino-2-phenylindole (DAPI), 5-hydroxytryptamine (5HT), choline acetyltransferase (ChAT), and neurokinin-1 (NK1) receptors. Injection coordinates were compared to coordinates of naloxone injections in the same study. Results are presented as mean ± SD.

In 4 animals, the caudal edge of the CMR was located in the midline, 0.2±0.7mm rostral to obex, 2.3±0.8mm deep (ventral to the dorsal surface). The preBC was located 1.8±0.8mm rostral from obex, 3.2±0.6mm lateral from midline, and 3.5±0.5mm deep. The medial medullary raphe was located at midline, 4.3±1.0mm rostral to obex, and 4.1±0.6mm deep. The corresponding coordinates for microinjections for the CMR were 0.4±0.6mm rostral and 4.1±0.6mm deep; for the preBC 2.3±0.6mm rostral, 2.7±0.4mm lateral, and 4.8±0.6mm deep; for the medial medullary raphe 5.1±0.6mm rostral and 7.0±0.8mm deep. Serotonergic neurons were observed in the raphe pallidus and raphe obscurus over the entire length of the CMR, NK1 receptors were found in the preBC, the retrotrapezoid nucleus, and the CMR.

The histological imaging verified that the naloxone injections were located in the caudal medullary raphe. The discrepancies in measured dimensions were likely due to reduction in brainstem volume as a result of histological fixation.

1. Resp Physiol Neurobiol 2019, 260:37-52